Hao Sun[1]
School of Astronautics,
Northwestern Polytechnical University,
127 Youyi Road,
Xi'an, Shaanxi 710072, China;
Department of Mechanical Engineering,
Stevens Institute of Technology,
1 Castle Point Terrace,
Hoboken, NJ 07030
e-mail: hsun9@stevens.edu

Jianjun Luo
School of Astronautics,
Northwestern Polytechnical University,
127 Youyi Road,
Xi'an, Shaanxi 710072, China

Zhongjing Ren
Department of Mechanical Engineering,
Stevens Institute of Technology,
1 Castle Point Terrace,
Hoboken, NJ 07030

Ming Lu
Center for Functional Nanomaterials,
Brookhaven National Laboratory,
98 Rochester Street,
Upton, NY 11973

Dmytro Nykypanchuk
Center for Functional Nanomaterials,
Brookhaven National Laboratory,
98 Rochester Street,
Upton, NY 11973

Sundeep Mangla
Downstate Medical Center,
State University of New York,
450 Clarkson Avenue,
P.O. Box 1189,
Brooklyn, NY 11203-2098

Yong Shi[1]
Department of Mechanical Engineering,
Stevens Institute of Technology,
1 Castle Point Terrace,
Hoboken, NJ 07030
e-mail: yshi2@stevens.edu

Shape Memory Alloy Bimorph Microactuators by Lift-Off Process

This study aims to develop a new fabrication process to create high-precision patterned shape memory alloy (SMA) bimorph micro-actuators by the e-beam evaporation technique. To examine the effect of the annealing process on nitinol (NiTi) thin film characteristics, the as-deposited and annealed NiTi thin films are, respectively, investigated. X-ray diffraction (XRD) results demonstrate the crystallization of NiTi thin films after annealing at 600 °C. The transformation behaviors of NiTi thin films during heating and cooling are studied using the differential scanning calorimeter (DSC). Furthermore, scanning electron microscopy (SEM) images indicate that SMA bimorph micro-actuators with high-precision features can be fabricated by the lift-off process, without any wet or dry etching procedures, and their thermomechanical behaviors are experimentally verified by comparing them with that of finite element analysis simulation results.
[DOI: 10.1115/1.4048146]

Keywords: shape memory alloy, bimorph, microactuators, e-beam evaporation, annealing, X-ray diffraction, differential scanning calorimeter, microfabrication, NiTi, high-precision patterned, lift-off

1 Introduction

Over the years, micro-actuators have been widely applied in a variety of disciplines such as aerospace [1,2], biomedical field [3,4], and microrobotics [5–7] and require delicate handling of micro-objects and high-precision coordination in the micro-environment. For the past three decades, the rapid advancements of micro-electromechanical system (MEMS) techniques have enabled the research of an extensive range of miniaturized micro-actuators using MEMS fabrication methods. Based on the actuation principles, micro-actuators can be classified into electrostatic [8], piezo-electric [9], electromagnetic [10], thermal and shape memory alloy (SMA) [11]. SMA has attractive advantages compared to other actuation mechanisms such as high power density, large actuation force, large displacement range, low cost, resistance to corrosion, and biocompatibility [12]. These advantages make SMA the preferred material to fabricate micro-actuators in various specific applications [13–15], including endovascular surgery, neural interfaces, drug delivery, and intestinal obstruction.

[1]Corresponding authors.

Contributed by the Manufacturing Engineering Division of ASME for publication in the Journal of Micro- and Nano-Manufacturing. Manuscript received December 10, 2019; final manuscript received July 31, 2020; published online September 9, 2020. Assoc. Editor: Sourabh K. Saha.

Among various SMA materials, the NiTi SMA composition is commonly used.

Shape memory alloy actuators, however, have often been described as having a slow response speed, which is seen as a major hindrance for the broad implementation [16]. That long response time is caused by the slow heating and cooling speed of the SMA [17]. To overcome the drawback of SMA, NiTi thin films based on MEMS have been studied by Walker [18] in 1990. The actuators formed by NiTi thin films can not only provide larger forces over longer displacements but also possess the fast response speed due to the larger surface area to volume ratio of NiTi thin films [19]. In addition, the advancements of NiTi thin film micro-actuators have been further achieved with the number of applications, which have been developed in MEMS fields. For example, using NiTi thin films, microgrippers [20,21], micropumps [22,23], and micro-imaging sensors [24] have been presented and fabricated. In general, there are several deposition techniques to fabricate NiTi thin films, namely, radio frequency or direct current (DC) magnetron sputtering, pulse laser deposition, plasma enhanced chemical vapor deposition, and flash evaporation [25]. Researchers commonly characterize NiTi thin films formed by sputtering deposition methods [26,27]. However, it seems to be difficult to micromachine NiTi thin films with high-precision features. In many applications, very uniform micropatterns with precise small feature sizes are particularly required [28]. Based on the sputtering deposition methods, NiTi films are usually lithographically fabricated into patterns using wet etching procedures, which produce nonuniform micropatterns with the severe undercut [28]. To achieve micropatterns with smooth edges, an anisotropic dry etching method has been proposed. But the drawback of this method is the slow etching rate, which is unacceptable in many cases [29]. According to the research of metal thin film, the e-beam evaporation technique might be a potential approach to fabricate the very uniform micropatterns of NiTi thin films with high-precision features, combining with lift-off resist method [30]. To study the characteristic of NiTi thin films formed by the e-beam evaporation technique, Noh [31] deposited NiTi thin films using e-beam evaporation method instead of sputtering. However, NiTi thin film microstructures with high-precision features were not micromachined in that paper. Therefore, it is necessary to develop a new approach to fabricate high-precision patterned SMA micro-actuators formed by the e-beam evaporation to meet specific requirements in various fields.

In this paper, a novel fabrication process is proposed for producing NiTi-aluminum SMA bimorph micro-actuators. In order to achieve the high-precision features, the fabrication process is combined with the e-beam evaporation and lift-off resist methods. To be more specific, this paper demonstrates the feasibility to fabricate the high-precision patterned NiTi thin film microstructures using the e-beam deposition technique and examines the effect of annealing process on the crystallization of NiTi thin films. Furthermore, thermomechanical behaviors of SMA bimorph micro-actuators are experimentally verified and compared with that of finite element analysis simulation results. Such studies may, therefore, contribute to a cost-effective fabrication process for the microrobotics applications.

This paper is organized as follows. The fabrication and annealing processes of SMA bimorph micro-actuators are described first, followed by the characterization analysis of NiTi thin films formed by the e-beam evaporation. Then, thermomechanical behaviors of the SMA bimorph micro-actuators are studied, and finite element analysis (FEA) and experiments are carried out to validate the feasibility. Finally, some conclusions are drawn.

2 Sample Preparation

In this paper, a novel fabrication process for producing NiTi-aluminum SMA bimorph micro-actuators with high-precision features is presented. For every fabrication step, the approach used to construct the features is described.

Figure 1 separately illustrates that photolithography, e-beam evaporation, and lift-off resist methods produce patterned NiTi thin films with high-precision features (steps 1–8), and the microstructures are released from silicon substrates using isotropic XeF_2 dry etching technique (steps 9–11). It started by initially depositing aluminum thin films with 500 nm thickness using the photolithography and e-beam evaporation techniques. To improve the adhesion between the substrate surface and negative photoresists, a 4 in. P-type (110) silicon wafer was cleaned and preheated in the HMDS chamber at 150 °C for 15 min. Then, MaN1410, a typical negative photoresist, was spin-coated on the substrate. The parameters of the spin coater were set as 500 rpm for 8 s and then as 3000 rpm for 30 s to achieve a uniform distribution of photoresists with the thickness of 1 μm on the wafer. After spin-coating, the wafer was placed on a hot plate at 100 °C for 60 s to evaporate the solvent in the photoresists and then exposed to the g-line UV light on a Karl SUSS MA6 Mask Aligner (SUSS MicroTec Inc.,

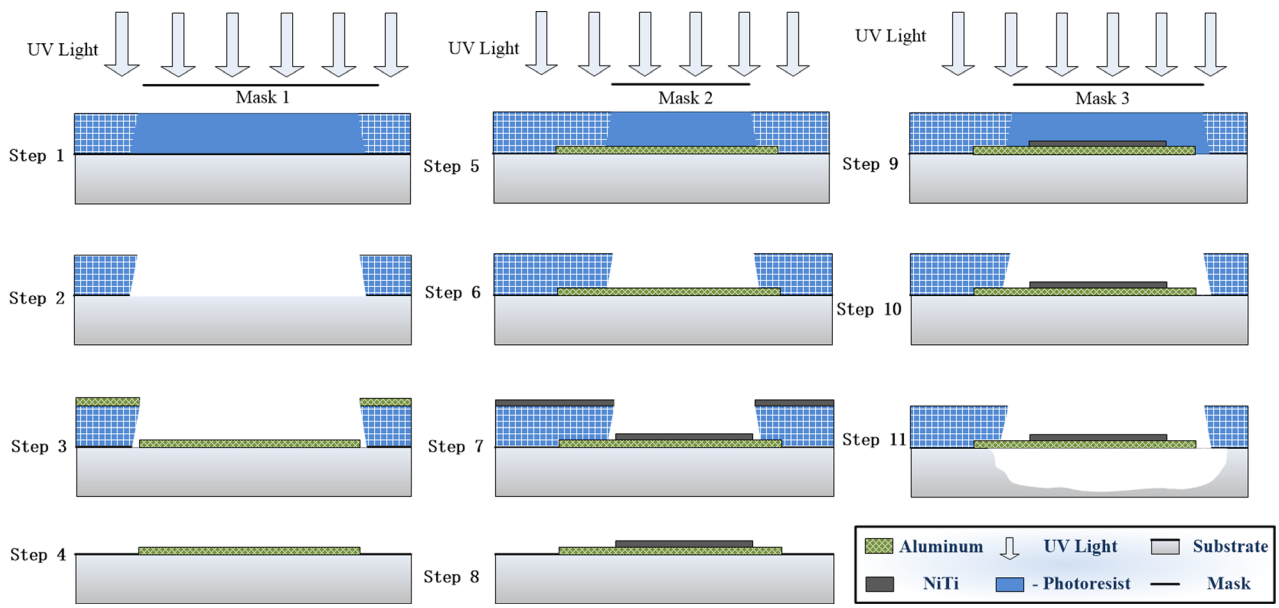

Fig. 1 Fabrication process using e-beam evaporation

Corona, CA) using Mask 1 for 40 s with a constant power of 10 mW/cm^2 (step 1), which was followed by development for 80 s in Mad 533/s, a metal ion-free TMAH based developer (step 2). After the development, the area of the removal negative photoresists formed the high-precision micropatterns of NiTi thin films. In order to fabricate NiTi-aluminum SMA bimorph micro-actuators, various planar patterns on the Mask 1 used for photolithography were designed. A graphite crucible with aluminum pellets was placed in the chamber for the e-beam deposition. Then, the deposition of 500 nm thickness aluminum thin films on the surface of substrate was carried out with a Kurt J. Lesker PVD 75 A machine (Kurt J. Lesker Company, Jefferson Hills, PA) (step 3). Since the e-beam deposition process needed low vacuum surroundings, it took about 4–5 h to pump the chamber down to a base pressure below 10^{-6} Torr. Then the rest of negative photoresists, as well as the aluminum film deposited on the surface of photoresists, was lifted-off in the strong organic PG remover solvent 1165 for 60 min at 80 °C, and the patterned aluminum structures were retained thanks to the perfect directivity of the e-beam deposition technique (step 4). Consequently, near-equiatomic patterned NiTi thin films with the thickness of 500 nm were deposited on the surface of aluminum layer with a similar fabrication process to construct NiTi-aluminum bimorph structures, and the minimum feature size involved was about 1 μm (steps 5–8). During the e-beam deposition process, the accelerating voltage and e-beam current were, respectively, maintained at 7.8 kV and 167 mA. At these conditions, the deposition rate of NiTi thin films was 0.06 nm/s. In order to release the bimorph microstructures from the substrate, but keep the contact pads fixed on the wafer, a MaN1410 negative photoresist was spin-coated and developed on the surface of the silicon wafer via the similar photolithography technique (steps 9 and 10, 1000 rpm for 30 s with 2 μm thickness, 10 mW/cm^2 UV light for 60 s with Mask 3 and develop in Mad 533/S for 80 s). The exposed silicon material was then etched using XeF_2 by the isotropic dry etching technique (step 11, etching rate was approximately 60 s to etch 0.5 μm thickness of silicon material at 3.5 Torr). The negative photoresists were used as dry etching masks to improve the efficiency of silicon etching. Finally, SMA bimorph micro-actuators were crystallized in a quartz tube furnace to perform the annealing process, as shown in Fig. 2. At first, a vacuum pump was used to remove the air inside the quartz tube. Then the vacuum pump was turned off, and argon was employed to make the quartz tube oxygen free. To avoid oxidation of NiTi thin films, this procedure was repeated three times. At last, the heater was turned on with a heating rate of 600 °C/h. Once reaching the desired annealing temperature of 600 °C, the temperature was kept constant for 1 h, and then, the heater was turned off to obtain a natural cooling procedure.

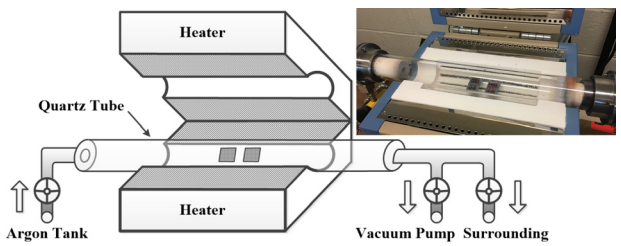

Fig. 2 Schematic setup of quartz tube furnace with argon overflow

3 Results and Discussion

3.1 Fabricated Patterns. Scanning electron microscopy (SEM) images (Hitachi S-4800, Hitachi High-Tech Company, Schaumburg, IL) were utilized to evaluate the high-precision patterned NiTi micro-actuators. Figures 3(*a*)–3(*c*) show SEM images of patterned NiTi thin film microstructures obtained by the fabrication process proposed in this paper. Both the low magnification and high magnification SEM images were taken after releasing NiTi microstructures from the silicon substrates using XeF_2 dry etcher. In addition, Fig. 3(*c*) illustrates that even in the features with sharp corners, this fabrication process produces quite smooth and relatively robust micropatterns. Furthermore, thanks to the perfect unique reactivity of silicon material using XeF_2, these NiTi micropatterns do not induce the fracture or tearing problems reported after releasing from the silicon wafer [28]. Since this fabrication procedure is combined with lift-off resist and the e-beam evaporation methods, the limit of fabrication precision is attributed to the photolithography technique, which depends on the UV wavelength utilized during the exposure process.

3.2 Material Characterization. In this study, to examine the effect of annealing process on NiTi thin film characteristics, the as-deposited and annealed NiTi thin films were, respectively, investigated. A Rigaku Ultima III X-ray diffractometer (Applied Rigaku Technologies Inc., Austin, TX) was employed at room temperature to determine the crystalline structures of NiTi thin films. Figure 4(*a*) illustrates the X-ray diffraction (XRD) test results of as-deposited NiTi thin films without annealing process. It is obvious that the results exhibit only one strong peak ($2\theta = 45$ deg), which can be identified as NiTi monoclinic structure (111) (martensite B19'), indicating that the as-deposited films are amorphous in nature. Subsequently, as shown in Fig. 4(*b*), it can be found that the annealing process shows a great influence on the XRD results. For annealed NiTi thin films, three strong peaks in total are observed, one peak ($2\theta = 42.5$ deg) corresponds NiTi

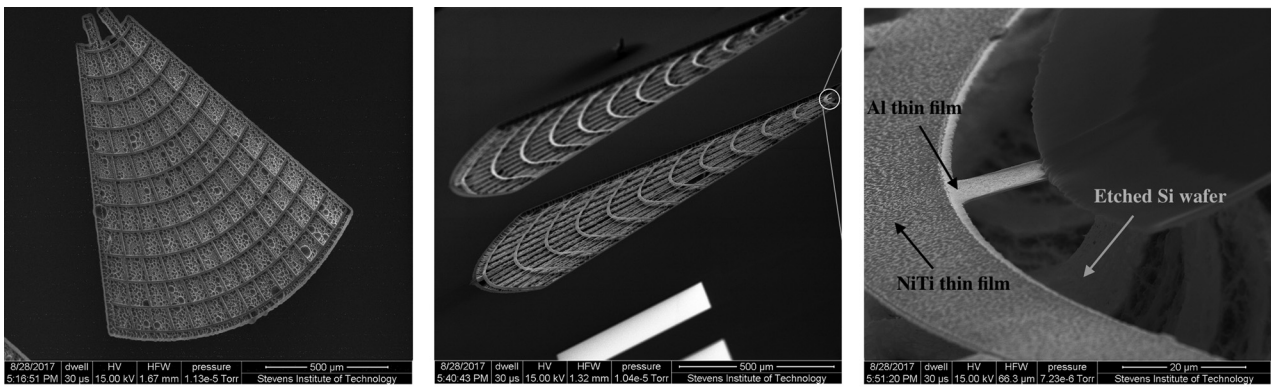

Fig. 3 SEM images of high-precision patterned NiTi thin films microstructures obtained using the fabrication process proposed in this paper: (*a*) top view, (*b*) lateral view, and (*c*) high magnification

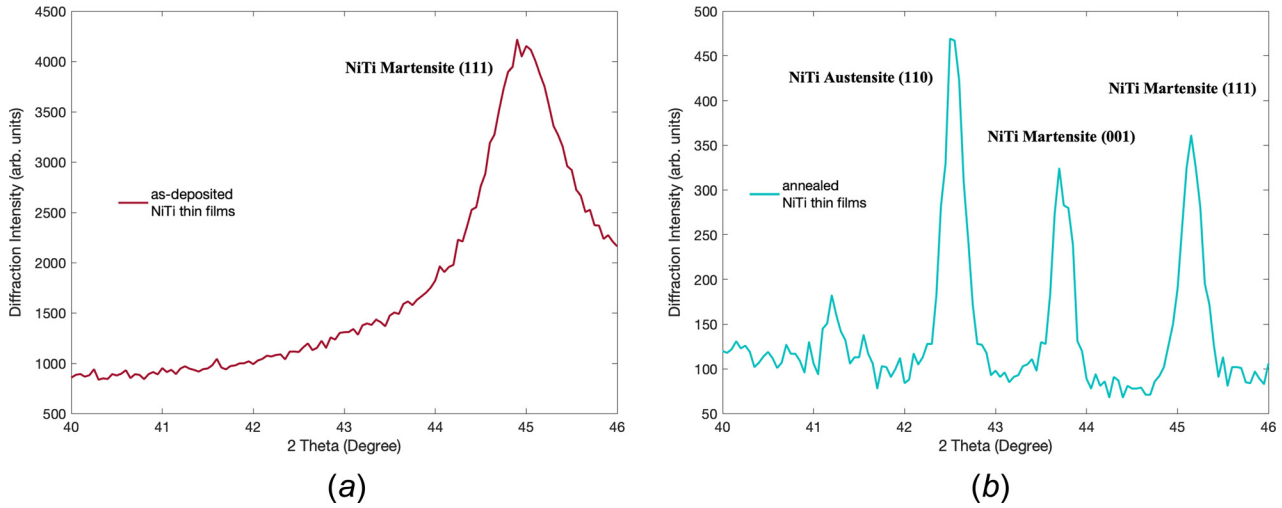

Fig. 4 XRD results of NiTi thin films: (*a*) as-deposited and (*b*) annealed

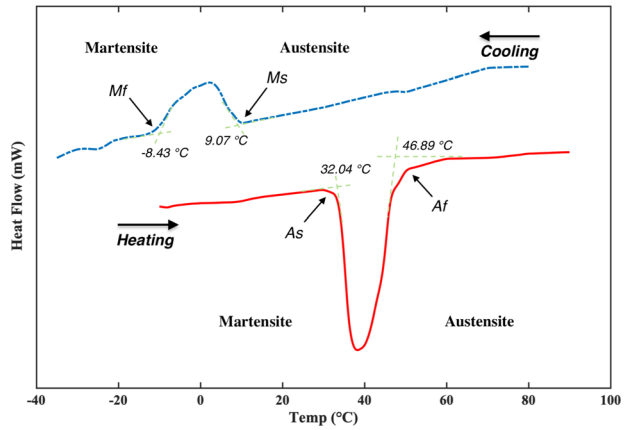

Fig. 5 DSC results of the annealed NiTi thin films

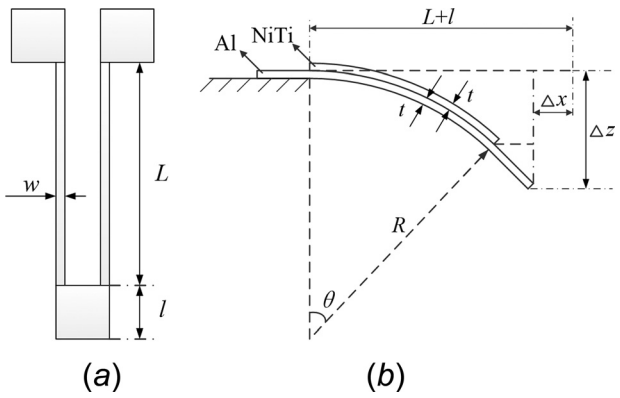

Fig. 6 Schematic drawing of bimorph micro-actuator structure: (*a*) top view and (*b*) cross section view after bending down

cubic structure (110) (austenite B2), and the other two peaks ($2\theta = 43.7$ deg and 45 deg) are identified as (111) and (001) NiTi monoclinic structure (martensite B19'), which reveals that austenite and martensite co-existed in the same annealed NiTi thin films at room temperature. The XRD results demonstrate that crystallization can be clearly detected when NiTi thin films annealed at 600 °C.

The transformation behaviors of NiTi thin films during heating and cooling were studied using the differential scanning calorimeter (DSC). Figure 5 shows the DSC results of the annealed NiTi thin films. The symbols A_s, A_f, M_s, and M_f indicate the starting and finishing temperatures of austenitic and martensitic phase-transformation. During the heating process, one endothermic peak corresponding to a martensite to austenite phase-transformation is observed. The starting and finishing temperatures (A_s and A_f) of austenitic phase-transformation are determined to be 32.04 °C and 46.89 °C. The transformation temperatures of A_s and A_f, above room temperature, which can be used as the thermal actuation command of the SMA actuators, will be beneficial to apply NiTi films in the micro-actuators.

3.3 Shape Memory Alloy Bimorph Micro-Actuator. Following successful e-beam deposition of patterned NiTi thin films, aluminum was used as the stress layer for the fabrication of NiTi-aluminum bimorph micro-actuators. A schematic NiTi-Al SMA bimorph micro-actuator structure is shown in Fig. 6. The micro-actuator has two legs, $10 \times 200\,\mu m^2$, connected with a $50 \times 50\,\mu m^2$ square-pad at a free end and two fixed contact pads at the other. The multilayer metals were deposited and bonding together naturally during the e-beam deposition processes. The aluminum was used as the bottom layer with the thickness of 0.5 μm and NiTi as the top layer of the bimorph structure, as well as with the thickness of 0.5 μm. In addition, there were two microrulers next to the legs of the micro-actuator. These microrulers helped to measure the planar displacement of the micro-actuators when thermally actuated. The metals vapored from the crucibles were deposited on the wafer at a quite low temperature (almost 75 °C), thanks to the cooling system employed in the vacuum chamber during the deposition process. After the deposition of NiTi and aluminum thin films, the temperature change of 55 °C between room temperature (20 °C) and physical vapor deposition (PVD) machine induced the residual thermal stress throughout the whole structures of SMA bimorph micro-actuators. Therefore, with the combination of NiTi and aluminum, the bending of the bimorph micro-actuator occurred after releasing it from silicon wafer following XeF_2 etching process, due to the mismatch in coefficient of thermal extension (CTE) of these two different materials. The radius of curvature R of the bent bimorph micro-actuator, could be expressed as

$$R = \frac{(w_1 E_1 t_1^2)^2 + (w_2 E_2 t_2^2)^2 + 2 w_1 w_2 E_1 E_2 t_1 t_2 (2t_1^2 + 3t_1 t_2 + 2t_2^2)}{6 w_1 w_2 E_1 E_2 t_1 t_2 (t_1 + t_2)(a_1 - a_2)\Delta T} \quad (1)$$

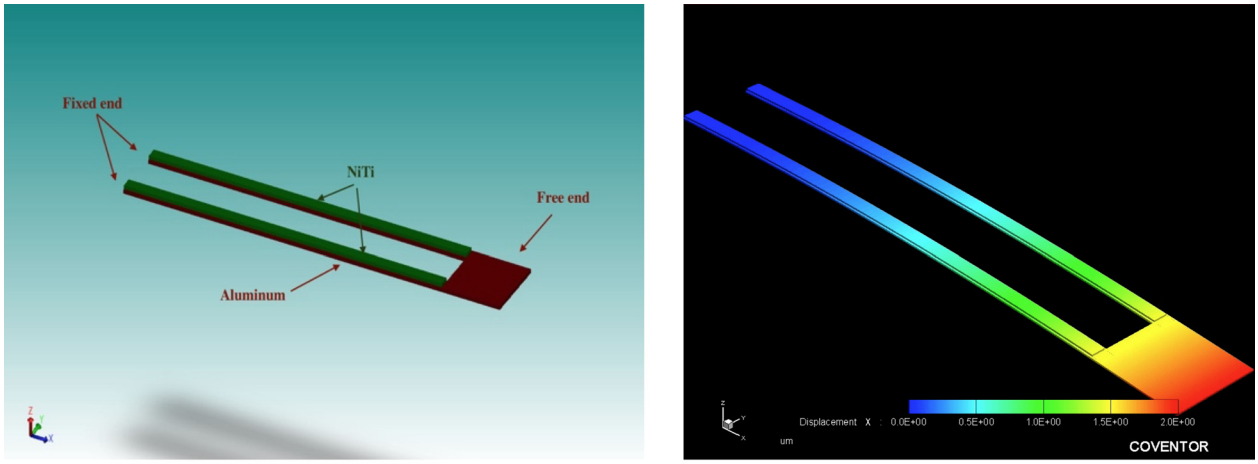

(*a*) (*b*)

Fig. 7 Thermomechanical behaviors of SMA bimorph micro-actuators investigated using the FEA method via coventor ware: (*a*) SMA bimorph micro-actuators model and (*b*) thermomechanical simulation result

where α is CTE of the materials, E is Young's modulus of the materials, t is the thickness of the layer, w is the width of the beam, ΔT is the temperature change, and subscripts 1 and 2 represent the NiTi and the aluminum layer, respectively [32]. When the parameters of the bimorph actuator are determined, the R is the function of temperature change ΔT

$$R = f(\Delta T) \tag{2}$$

In addition, the radius of curvature R, the bending angle θ (in radian), and the length of the beam L have the following relationship:

$$\theta = \frac{L}{R} \tag{3}$$

Meanwhile, as shown in Fig. 6, the bending of the bimorph micro-actuator formed the planar displacement Δx and the vertical displacement Δz, along the x-direction and z-direction, respectively. According to the geometry theory, the geometry relationship between displacement Δx, Δz, and the bending angle θ can be expressed as

$$\begin{aligned}\Delta x &= \Delta L_x + \Delta l_x \\ &= L - L\cos\frac{\theta}{2} + l - l\cos\theta\end{aligned} \tag{4}$$

$$\begin{aligned}\Delta z &= \Delta L_z + \Delta l_z \\ &= L\sin\frac{\theta}{2} + l\sin\theta\end{aligned} \tag{5}$$

Combining equations (1), (2), (3), and (4), the displacement Δx of the bimorph micro-actuator along the x-direction due to the thermal effect from a temperature change becomes

$$\begin{aligned}\Delta x &= L - L\cos\left(\frac{L}{2R}\right) + l - l\cos\left(\frac{L}{R}\right) \\ &= L - L\cos\left(\frac{L}{2f(\Delta T)}\right) + l - l\cos\left(\frac{L}{f(\Delta T)}\right) \\ &= g(\Delta T)\end{aligned} \tag{6}$$

Combining equations (1), (2), (3), and (5), the displacement Δz of the bimorph micro-actuator along the z-direction due to the thermal effect from a temperature change becomes

Table 1 Thermomechanical properties of NiTi and Al

Properties	NiTi	Al
CTE (10^{-6} 1/K)	6.6 (Martensite) 11 (Austenite)	23.1
Density (g/cm^3)	6.45	2.7
Young's modulus (GPa)	80	70
Poisson's ratio	0.3	0.35

$$\begin{aligned}\Delta z &= L\sin\left(\frac{L}{2R}\right) + l\sin\left(\frac{L}{R}\right) \\ &= L\sin\left(\frac{L}{2f(\Delta T)}\right) + l\sin\left(\frac{L}{f(\Delta T)}\right) \\ &= h(\Delta T)\end{aligned} \tag{7}$$

Then, the thermomechanical behaviors of SMA bimorph micro-actuators were investigated using the FEA method via Coventor Ware. As shown in Fig. 7(*a*), the SMA bimorph micro-actuator finite element models are built, with one end fixed and one end free. The bottom parts are the main body of micro-actuators using the aluminum material, and the other parts employ as the top layer using NiTi thin films to induce residual stress throughout the whole structure to make this bimorph micro-actuators bend. To determine the displacement of bimorph SMA micro-actuator along the x-direction and z-direction due to the thermal effect from a temperature change ($\Delta T = 55$ K), FEA simulations were performed using the thermomechanical properties as shown in Table 1. As a result, Fig. 7(*b*) shows the maximum displacement Δx (1.98 μm) and Δz (29.91 μm) of the micro-actuator when the temperature decreased from 75 °C to 20 °C.

Figures 8(*a*) and 8(*b*), respectively, show the bimorph SMA micro-actuators before and after a dry etching process observed by an optical microscope. Before releasing from the silicon wafer, as shown in Fig. 8(*a*), the whole microstructure is fixed. Following the XeF_2 etching process, the SMA bimorph micro-actuator was released from silicon, as shown in Fig. 8(*b*), and the significant bending result can be observed. The maximum displacement Δx (2 μm) of the micro-actuator can be measured with the help of microrulers deposited next to the microstructures. According to Eq. (6), we can calculate the temperature change $\Delta T = 55.4$ K. Finally, the displacement Δz (30.13 μm) of the bimorph micro-actuator along the z-direction can be calculated using Eq. (7),

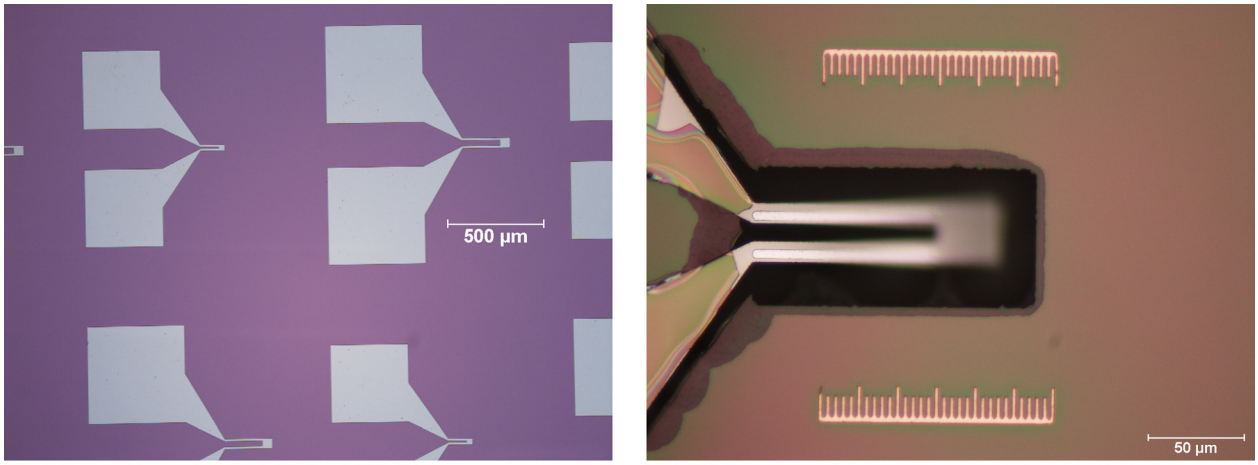

(*a*) (*b*)

Fig. 8 Optical microscopy images of bimorph SMA micro-actuators before and after dry etching process: (*a*) before a dry etching process and (*b*) after a dry etching process

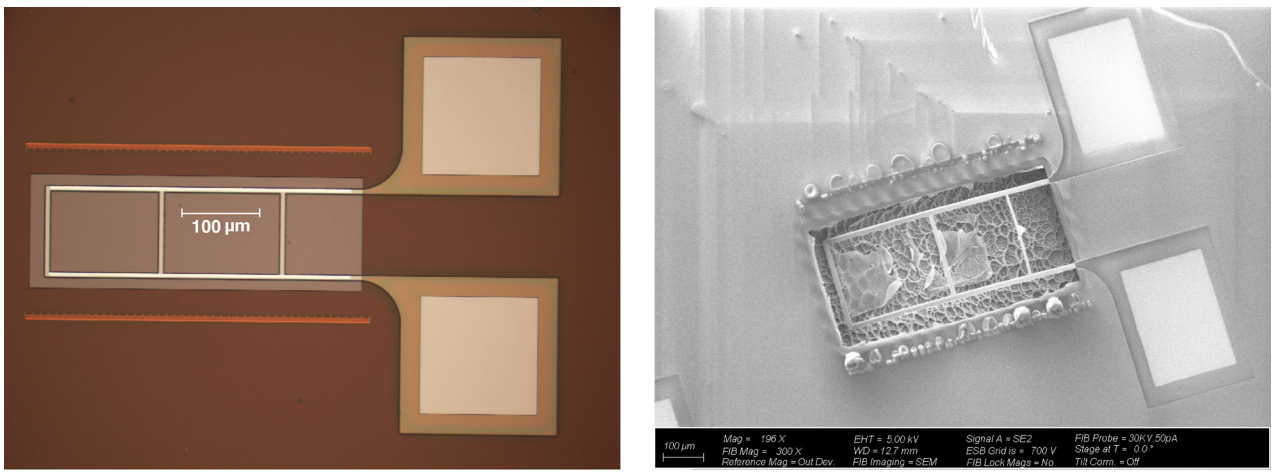

(*a*) (*b*)

Fig. 9 Bimorph SMA micro-actuator: (*a*) optical microscopy picture and (*b*) SEM picture

without any additional measurement of Δz, which is experimentally verified compared with FEA simulation results.

Furthermore, Figs. 9(*a*) and 9(*b*) show the optical microscopy picture and SEM picture of the same bimorph SMA micro-actuator in the static response experiment, which demonstrate the feasibility to fabricate NiTi SMA micro-actuator using the novel deposition process proposed in this paper.

4 Conclusion

NiTi films formed by the sputtering techniques are usually lithographically fabricated into patterns using wet or dry etching procedures, which produce nonuniform micropatterns with severe undercut, as well as slow etching rate problems. In this paper, aiming to solve the above problems, a novel fabrication process combined with the e-beam evaporation and lift-off resist techniques has been evaluated, which can fabricate SMA micro-actuators with high-precision features. Meanwhile, the effect of the annealing process on the crystallization of NiTi thin films has been examined. The following conclusions can be drawn. The as-deposited films formed by e-beam evaporation are amorphous in nature, and crystallization of NiTi thin films can be clearly detected after annealing at 600 °C. The phase-transformation temperatures, which can provide the thermal actuation command of the proposed SMA actuators, have been determined above room temperature based on the DSC results. Furthermore, the SMA bimorph micro-actuators have been successfully fabricated, and their thermomechanical behaviors have been experimentally verified and compared with FEA simulation results. Our work may contribute to a cost-effective fabrication process for the microrobotics applications.

Acknowledgment

Hao Sun acknowledges support from National Key Laboratory of Aerospace Flight Dynamics, Northwestern Polytechnical University, China, and also from Department of Mechanical Engineering, Stevens Institute of Technology, U.S. The authors most gratefully appreciate funding provided for this work by the Stevens NPU Ph.D. Program from China Scholarship Council. Also, this research used resources of the Center for Functional Nanomaterials, which is a U.S. DOE Office of Science Facility, at Brookhaven National Laboratory under Contract No. DE-SC0012704.

Funding Data

- China Scholarship Council (Funder ID: 10.13039/501100004543).
- U.S. Department of Energy, Office of Science, Basic Energy Sciences (Contract No. DE-SC0012704; Funder ID: 10.13039/100000015).

Nomenclature

E_1 = the Young's modulus of NiTi, Pa
E_2 = the Young's modulus of Al, Pa
l = the length of the square-pad, m
L = the length of the beam, m
R = the curvature radius of the bent bimorph microactuator, m
t_1 = the total thickness of the NiTi layer in microactuator, m
t_2 = the total thickness of the Al layer in microactuator, m
w_1 = the width of the beam formed by NiTi, m
w_2 = the width of the beam formed by Al, m
α_1 = the coefficient of thermal extension of NiTi in microactuator, 10^{-6} 1/K
α_2 = the coefficient of thermal extension of Al in microactuator, 10^{-6} 1/K
ΔT = the temperature change, K
Δx = the planar displacement of the bimorph microactuator along the x-direction, m
Δz = the vertical displacement of the bimorph microactuator along the z-direction, m
θ = the bending angle of the bent bimorph microactuator, rad

References

[1] Barbarino, S., Flores, E. I. S., Ajaj, R. M., Dayyani, I., and Friswell, M. I., 2014, "A Review on Shape Memory Alloys With Applications to Morphing Aircraft," Smart. Mater. Struct., **23**(6), p. 063001.
[2] Kudva, J. N., 2004, "Overview of the DARPA Smart Wing Project," J. Intell. Mater. Syst. Struct., **15**(4), pp. 261–267.
[3] Boyvat, M., Koh, J., and Wood, R. J., 2017, "Addressable Wireless Actuation for Multijoint Folding Robots and Devices," Sci. Robot., **2**(8), p. eaan1544.
[4] Booth, J. W., Shah, D., Case, J. C., White, E. L., Yuen, M. C., Cyr-Choiniere, O., and Kramer-Bottiglio, R., 2018, "OmniSkins: Robotic Skins That Turn Inanimate Objects Into Multifunctional Robots," Sci. Robot., **3**(22), p. eaat1853.
[5] Seok, S., Onal, C. D., Cho, K., Wood, R. J., Rus, D., and Kim, S., 2013, "Meshworm: A Peristaltic Soft Robot With Antagonistic Nickel Titanium Coil Actuators," IEEE-ASME Trans. Mech., **18**(5), pp. 1485–1497.
[6] Song, S., Lee, J., Rodrigue, H., Choi, I., Kang, Y. J., and Ahn, S., 2016, "35 Hz Shape Memory Alloy Actuator With Bending-Twisting Mode," Sci. Rep., **6**, p. 21118.
[7] Laschi, C., Mazzolai, V., and Cianchetti, M., 2016, "Soft Robotics: Technologies and Systems Pushing the Boundaries of Robot Abilities," Sci. Robot., **1**(1), p. eaah3690.
[8] De Jong, B. R., Brouwer, D. M., De Boer, M. J., Jansen, H. V., Soemers, H. M., and Krijnen, G. J., 2010, "Design and Fabrication of a Planar Three-DOFs MEMS-Based Manipulator," J. Microelectromech. Syst., **19**(5), pp. 1116–1130.
[9] Liang, Q., Zhang, D., Chi, Z., Song, Q., Ge, Y., and Ge, Y., 2011, "Six-DOF Micro-Manipulator Based on Compliant Parallel Mechanism With Integrated Force Sensor," Robot. Comput. Integr. Manuf., **27**(1), pp. 124–134.
[10] Lin, S., Chang, S., and Li, B., 2014, "Gearshift Control System Development for Direct-Drive Automated Manual Transmission Based on a Novel Electromagnetic Actuator," Mechatronics, **24**(8), pp. 1214–1222.
[11] Nespoli, A., Besseghini, S., Pittaccio, S., Villa, E., and Viscuso, S., 2010, "The High Potential of Shape Memory Alloys in Developing Miniature Mechanical Devices: A Review on Shape Memory Alloy Mini-Actuators," Sensor Actuators A, **158**(1), pp. 149–160.
[12] Jani, J. M., Leary, M., Subic, A., and Gibson, M. A., 2014, "A Review of Shape Memory Alloy Research, Applications and Opportunities," Mater. Des., **56**, pp. 1078–1113.
[13] Spiotta, A. M., Chaudry, M. I., Hui, F. K., Turner, R. D., Kellogg, R. T., and Turk, A. S., 2015, "Evolution of Thrombectomy Approaches and Devices for Acute Stroke: A Technical Review," J. Neurointerventional Surg., **7**(1), pp. 2–7.
[14] Heller, L., Vokoun, D., Sittner, P., and Finckh, H., 2012, "3D Flexible NiTi-Braided Elastomer Composites for Smart Structure Applications," Smart Mater. Struct., **21**(4), p. 045016.
[15] Nisar, A., Afzulpurkar, N., Mahaisavariya, B., and Tuantranont, A., 2008, "MEMS-Based Micropumps in Drug Delivery and Biomedical Applications," Sensor Actuators B, **130**(2), pp. 917–942.
[16] Stachiv, I., Sittner, P., Olejnicek, J., Landa, M., and Heller, L., 2017, "Exploiting NiTi Shape Memory Alloy Films in Design of Tunable High Frequency Microcantilever Resonators," Appl. Phys. Lett., **111**(21), p. 213105.
[17] Lee, H. T., Kim, M. S., Lee, G. Y., Kim, C. S., and Ahn, S. H., 2018, "Shape Memory Alloy (SMA)-Based Microscale Actuators With 60% Deformation Rate and 1.6 kHz Actuation Speed," Small, **14**(23), p. 1801023.
[18] Walker, J. A., Gabriel, K. J., and Mehregany, M., 1990, "Thin-Film Processing of TiNi Shape Memory Alloy," Sensor Actuators A, **21**(1–3), pp. 243–246.
[19] Choudhary, N., and Kaur, D., 2016, "Shape Memory Alloy Thin Films and Heterostructures for MEMS Applications: A Review," Sensor Actuators A, **242**, pp. 162–181.
[20] Wongweerayoot, E., Srituravanich, W., and Pimpin, A., 2015, "Fabrication and Characterization of Nitinol-Copper Shape Memory Alloy Bimorph Actuators," J. Mater. Eng. Perform., **24**(2), pp. 635–643.
[21] Fu, Y. Q., Luo, J. K., Ong, S. E., Zhang, S., Flewitt, A. J., and Milne, W. I., 2008, "A Shape Memory Microcage of TiNi/DLC Films for Biological Applications," J. Micromech. Microeng., **18**(3), p. 035026.
[22] Makino, E., Mitsuya, T., and Shibata, T., 2001, "Fabrication of TiNi Shape Memory Micropump," Sensor Actuators A, **88**(3), pp. 256–262.
[23] Sassa, F., Al-Zain, Y., Ginoza, T., Miyazaki, S., and Suzuki, H., 2012, "Miniaturized Shape Memory Alloy Pumps for Stepping Microfluidic Transport," Sensor Actuators B, **165**(1), pp. 157–163.
[24] Chung, C. Y., and Chan, P. M., 2011, "NiTi Shape Memory Alloy Thin Film Micro-Cantilevers Array," Thin Solid Films, **519**(15), pp. 5307–5309.
[25] Fu, Y., Du, H., Huang, W., Zhang, S., and Hu, M., 2004, "TiNi-Based Thin Films in MEMS Applications: A Review," Sensor Actuators A, **112**(2–3), pp. 395–408.
[26] Huang, X., and Ramirez, A. G., 2009, "Effects of Film Dimension on the Phase Transformation Behavior of NiTi Thin Films," Appl. Phys. Lett., **95**(10), p. 101903.
[27] Rios, S., Karaman, I., and Zhang, X., 2010, "Crystallization and High Temperature Shape Memory Behavior of Sputter-Deposited NiMnCoIn Thin Films," Appl. Phys. Lett., **96**(17), p. 173102.
[28] Chun, Y. J., Levi, D. S., Mohanchandra, K. P., Fishbein, M. C., and Carman, G. P., 2010, "Novel Micro-Patterning Processes for Thin Film NiTi Vascular Devices," Smart Mater. Struct., **19**(10), p. 105021.
[29] Zamponi, C., Rumpf, H., Schmutz, C., and Quandt, E., 2008, "Structuring of Sputtered Superelastic NiTi Thin Films by Photolithography and Etching," Mater. Sci. Eng. A, **481–482**, pp. 623–625.
[30] Ren, Z., Yuan, J., Su, X., Sun, H., Galos, R., Shi, Y., Mangla, S., Lu, M., and Camino, F., 2019, "Vertical Deployment of Multilayered Metallic Microstructures With High Area-to-Mass Ratios by Thermal Actuation," ASME J. Micro-Nano-Manuf., **7**(3), p. 031002.
[31] Noh, H. Y., Lee, K. H., Cui, X. X., and Choi, C., 2000, "The Composition and Structure of NiTi Thin Film Formed by Electron Beam Evaporation," Scr. Mater., **43**(9), pp. 847–852.
[32] AbuZaiter, A., Nafea, M., and Ali, M. S. M., 2016, "Development of a Shape-Memory-Alloy Micromanipulator Based on Integrated Bimorph Microactuators," Mechatronics, **38**, pp. 16–28.